Extraction of Heat Transfer Macromodels for MEMS Devices

Che-Chia Yu and Yao-Joe Yang
Department of Mechanical Engineering
National Taiwan University
1 Roosevelt Rd. Sec 4., 106, Taipei, Taiwan, ROC
carte@mems.me.ntu.edu.tw

Abstract

A model order reduction (MOR) technique for heat-transfer system-level modeling is presented. A heat transfer solver using the finite difference method (FDM), which is appropriate for MEMS thermal analysis, is implemented. The numerical models generated by the FDM solver then were successfully reduced into low-order compact models by an Arnoldi-based model-order-reduction technique. The compact macromodels can be easily inserted into system-level or circuit simulators. We also demonstrated that the macromodel results for a thermal actuator are in good agreement with the experimental results.

1. Introduction

There are numerous heat transfer applications in MEMS, such as thermal actuating, uncooled infrared sensing, chip cooling, temperature sensing, PCR, and so on. Most of the applications need feedback loops for precise control or actuation, and thus require compact but accurate heat transfer models for system-level analysis. The typical approach for creating heat-transfer compact models is to use lumped-element methods [1]. For example, a lumped constant heat capacity (C_{th}) can be used to represent an average heat capacity for a complex geometry, and lumped heat resistors (R_{th}) can be used to account for each energy leakage mechanism, including conduction, convection, and radiation. Although this approach significantly simplifies complex heat transfer systems, it required many costly FEM (or FDM) simulations to extract C_{th} and R_{th}, and the accuracy of lumped-element models is detrimentally affected by the complexity of original geometries.

In this work, we implemented a 3-D FDM heat transfer solver, and demonstrated that the numerical models created by FDM/FEM heat transfer solvers can be transformed into compact macromodels using an Arnoldi-based model order reduction (MOR) technique [2-4]. Because the compact macromodels are generated from the FEM/FDM approximation of complex geometries, they preserve the original geometric characteristics. Also, since the order of compact macromodels is much less than original FEM/FDM models, the total computational time is significantly reduced by at least 3 orders of magnitude. This performance improvement thus makes the compact macromodels compatible for system-level or circuit simulations, which is essential for overall performance prediction.

2. Theory

2.1 *Heat Transfer Governing Equations*

In this study, we focus on the heat transfer effect of MEMS structures with various boundary conditions. The governing equation of 3D transient heat-transfer problem is the so-called heat equation [5]:

$$\nabla^2 T + \frac{1}{k} g(\vec{r},t) = \frac{1}{\alpha}\frac{\partial T}{\partial t}; \quad \text{Region } \boldsymbol{R},\ t>0 \qquad (1)$$

where T is temperature distribution, $\boldsymbol{R}$ is the computational domain (MEMS structure), $g(\vec{r},t)$ is the heat generated per unit volume in the position $\vec{r}$, $\alpha\,(=\frac{k}{\rho c})$ is thermal diffusivity, ρ is density, c is specific heat, and k is thermal conductivity. The boundary and initial conditions are

$$k_i \frac{\partial T}{\partial n_i} + h_i T = f_i(\vec{r},t) \quad \text{Boundary } S_i,\ t>.0 \qquad (2)$$

$$T(\vec{r},t) = F(\vec{r}) \qquad \text{Region } \boldsymbol{R},\ t=0 \qquad (3)$$

where $F(\vec{r})$ is the initial temperature, $f_i(\vec{r},t)$ is the heat flux flowing out of the boundary S_i, k_i is thermal conductivity on the boundary S_i, h_i is the convection coefficient on the boundary S_i.

The heat transfer governing equations can be approximated using the finite-element method (FEM) or the finite-difference method (FDM). In this work, we develop a 3D transient heat transfer solver with FDM approximation on Equations 1, 2 and 3 [6]. Since the operation temperatures for most of MEMS devices are relatively low, the radiation effect is very small and is not considered in the FDM solver.

2.2 *Methodology of Model Order Reduction (MOR)*

Although the 3-D FDM heat transfer solver is capable of calculating transient behaviors, the computational cost is very expensive due to the significant large number of nodes in the 3-D computational domain. Fortunately, the governing equation as well as the boundary conditions, as shown in Equations 1 and 2, are linear equations, and therefore the system matrices generated by the FDM or FEM approximation process for Equations 1 and 2 can be reduced by an Arnoldi-based model order reduction technique. The detailed description of the model order reduction process is described as follows:

0-7803-7731-1/03/$17.00 ©2003 IEEE

The dynamic system equation formulated by the FDM approximation of governing equation (Equation 1) and the boundary conditions (Equation 2) can be written as:

$$\dot{\bar{x}} = \underline{\underline{A}}\bar{x} + \underline{\underline{B}}\bar{u}$$
$$\bar{y} = \underline{\underline{C}}^T\bar{x} + \underline{\underline{D}}\bar{u} \quad (5)$$

where $\underline{\underline{A}}$ is an n by n matrix and n is the total number of nodes, $\bar{x}$ is the vector which contains the unknown temperature distribution on each node, and the input function $\bar{u}$, is the combination of $\bar{u}_1, \bar{u}_2, \bar{u}_3$ ...etc. $\bar{u}_1, \bar{u}_2, \bar{u}_3$ ...can be the heat generation, heat flux or constant temperature boundary conditions in the heat transfer system model. The matrices $\underline{\underline{C}}$ and $\underline{\underline{D}}$ are carefully chosen so that the output vector $\bar{y}$ can be designed as the average temperature of different components, the temperature distribution on a specific area, or even the tip displacement of a thermal actuator. In the *Laplace* domain, the transfer function of the system is:

$$T(s) = \underline{\underline{C}}^T(\underline{\underline{I}}s - \underline{\underline{A}})^{-1}\underline{\underline{B}} + \underline{\underline{D}}$$
$$= \underline{\underline{C}}^T(\underline{\underline{I}} - s\underline{\underline{A}}^{-1})^{-1}\underline{b} + \underline{\underline{D}} \quad (6)$$
$$\underline{b} = -\underline{\underline{A}}^{-1}\underline{\underline{B}}$$

After expanding the transfer function in Taylor series about $s=0$, we obtain:

$$T(s) = \underline{\underline{C}}^T(\underline{\underline{I}} + s\underline{\underline{A}}^{-1} + s^2\underline{\underline{A}}^{-2} + \ldots)\underline{b} = \sum_{k=0}^{\infty} m_k s^k$$

where m_k are the coefficients of the Taylor series, $(m_k = \underline{\underline{C}}^T(\underline{\underline{A}}^{-k})\underline{b})$. The Taylor expansion can be truncated to approximate the transfer function $T(s)$. However, $(\underline{\underline{A}}^{-k})\underline{b}$ lines up with a single eigenvector quickly and thus this procedure is usually numerically unstable. Therefore, we apply the Arnoldi-based algorithm to stably compute orthogonal bases $\{\bar{v}_i\}$ that spans the Krylov subspace:

$$K_q(\underline{\underline{A}}^{-1}, \underline{b}) = span\{\underline{b}, \underline{\underline{A}}^{-1}\underline{b}, \underline{\underline{A}}^{-2}\underline{b}, \cdots, \underline{\underline{A}}^{-(q-1)}\underline{b}\}$$

Given the matrix $\underline{\underline{V}}$ whose columns are $\{\bar{v}_i\}$, the reduced order model (macromodel) is

$$\dot{\bar{x}}_q = \underline{\underline{A}}_q\bar{x}_q + \underline{\underline{B}}_q\bar{u}$$
$$\bar{y} = \underline{\underline{C}}_q{}^T\bar{x}_q + \underline{\underline{D}}\bar{u} \quad (7)$$

where

$$\underline{\underline{A}}_q = \underline{\underline{v}}^T\underline{\underline{A}}\underline{\underline{v}} \quad \underline{\underline{B}}_q = \underline{\underline{v}}^T\underline{\underline{B}}$$
$$\underline{\underline{C}}_q = \underline{\underline{v}}^T\underline{\underline{C}} \quad (8)$$

Note that the reduced system, as shown in Equation 7, has the same input ($\bar{u}$) and output ($\bar{y}$) as in Equation 5. Since the typical ranks of $\underline{\underline{A}}_q$, $\underline{\underline{B}}_q$ and $\underline{\underline{C}}_q$ are very small, the computational efficiency for simulating transient responses and frequency responses of the macromodel is significantly increased.

3. Applications of the MOR Technique on MEMS Devices Modeling

The main purpose of MOR techniques is to reduce the order of the original FEM/FDM systems so that the computational performance will be improved with little compromise in accuracy. In this section, two examples of model-order-reduction applications on MEMS heat transfer effects are presented. The first example provides the estimation of the tip deflection of a thermal actuator based on the temperature calculation from the macromodels. Measured results are also demonstrated. The second example demonstrates the electric resistance variation of an infrared imager (bolometer) cell due to heat absorption. The macromodel results are also verified with our FDM solver and commercial FEM package Coventorware [7].

3.1 Thermal actuator

3.1.1 Comparison with the FEM/FDM Results

Figure 1 shows the CCD picture of thermal actuator which was fabricated by Multi-User MEMS Process (MUMPS) [8]. The device is fixed to the substrate at the anchors. With a constant electrical current flowing through the hot arm and the cold arm (when a constant voltage is applied across the two contact pads), the asymmetric dimension of two arms causes the current density of the hot arm to be larger than that of the cold arm. This asymmetric heating caused by current density will make the temperature in the hot arm higher than that in the cold arm. The thermal expansion difference between the two arms results in an in-plane bending of whole structure.

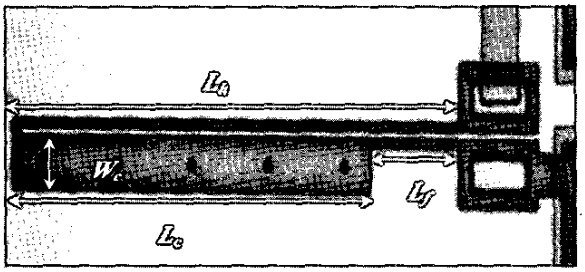

Figure 1: *The CCD picture of the experimental device. The contact pads are on the right side of the picture and are not completely shown.*

This thermal actuator is modeled by imposing several thermal boundary conditions and volume conditions on the structure. The convection boundaries are applied on the surfaces adjacent to the air. The constant-temperature boundaries are applied to the

interfaces between the anchors and the substrate. Volume heat generation (J/m^3) is applied on the whole structure, and the heat-generation value is determined by the electrical current density distribution, which can be easily accurately estimated by the effective resistance of each segment of the structure. The mechanical, thermal, and electric properties as well as the dimension of the measured and simulated device are listed in Table 1 and Table 2.

Geometrical dimensions	Length(μm)
Length of hot arm (L_h)	200
Width of hot arm (W_h)	3
Length of cold arm (L_c)	160
Width of cold arm (W_c)	16
Gap (g)	3
Length of flexure (L_f)	40
Width of flexure (W_f)	3
Thickness (t)	2

Table 1: *The dimensions of thermal actuator.*

Mechanical property	
Density ($kg/\mu m^3$)	2.23×10^{-15}
Thermal property	
thermal conductivity ($pW/\mu m \cdot K$)	1.48×10^{8}
specific heat ($pJ/kg \cdot K$)	1.0×10^{14}
convection coefficient ($pW/\mu m^2 \cdot K$)	5
Electrical property	
Resistance (*ohm/sq*)	10

Table 2: *The mechanical, thermal and electrical properties of thermal actuator.*

Figure 2 shows the simulated average temperatures of the thermal actuator vs. time from the FDM solver, the Coventorware FEM solver, and macromodels. The temperatures on the bottom surfaces of the anchors are fixed at 300K. The applied voltage across the contact pads is 3 volts. The convection coefficient for the surfaces under the convection boundary condition is $5\,(pW/\mu m^2 \cdot K)$. For the FDM model, the thermal actuator is meshed into 11127 nodes. For the Coventorware FEM model, the same structure is also meshed into 11127 nodes (linear brick elements) in order to analyze the error. These results not only indicate that our FDM solver in comparable to commercial FEM solver in terms of accuracy, but also indicate that the results calculated by the macromodel are in an excellent agreement with the FDM/FEM results.

Table 3 presents the comparison of the performance as well as the accuracy between the results by the FDM solver and by the macromodels with various orders. The results demonstrate that the macromodels give significant reductions in the computational cost, while sustain excellent accuracy compared with the full-meshes (FDM solver) result. For this MEMS thermal actuator, these preliminary numerical results show that the macromodels with order larger than 2 match the FDM/FEM results very well.

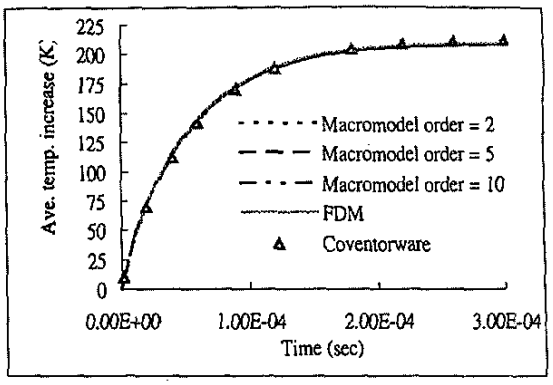

Figure 2: *Comparison of the FDM, the macromodel and Coventorware results for average temperature increase of thermal actuator.*

	Simulation time (sec)	Speed-up factor	Error (%)
MOR order = 2	<0.01	$>2\times10^{6}$	0.51
MOR order = 5	0.01	2×10^{6}	0.50
MOR order=10	0.44	4×10^{4}	0.50
FDM	18743.000		N/A

Table 3: *The performance comparison of FDM solver and macromodels.*

3.1.2 Comparison with the Measured Results

In this section, the measured tip deflection of the thermal actuator will be compared with the results estimated by the macromodel (order 5). In order to calculate the tip deflection based on the temperature distribution on the device, we apply the analytical equations derived in [9] and [10].

The comparison of the measured and calculated in-plane deflection of the actuator is shown in Figure 3. At the low temperature, the measured results match with the FDM solver and the macromodels very well. At high input voltage, the radiation heat become significant because of the high temperature induced by the joule heating. As a result, the simulated results deviate from the measured results at higher input voltages.

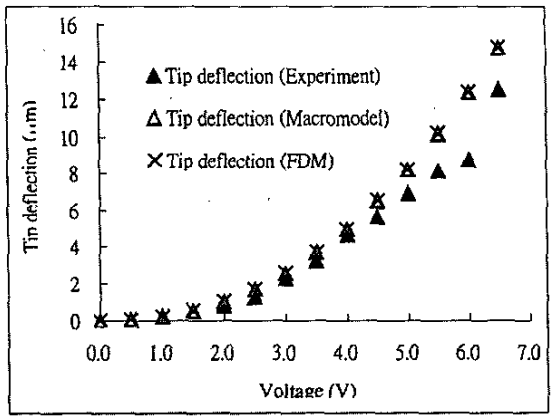

Figure 3: *Comparison of experimental tip displacement and macromodel calculated tip displacement with an input voltage from 1 volt to 6.5 volts.*

3.2 Infrared imager

Figure 4 shows a typical schematic of a pixel cell in an infrared imager [11]. This cell consists of a Si_3N_4 suspended structure (absorber) of 0.5 μm in thickness and two supporting tethers. A thin film of vanadium oxide (VO_x) is deposited on the suspended structure. The TCR (temperature coefficient of resistance) of the VO_x layer is -0.02/K (assumed the operating temperature is in linear range). The input heat flux impinging on the top of the absorber is 1000 pW/μm^2. The resistance variation caused by the temperature distribution of the absorber is obtained by carefully choosing the $\underline{\underline{C}}$ matrix. Figure 5 shows both the FDM and the macromodel results for the transient behavior of electrical resistance when the infrared imager pixel absorbs heat flux. The discrepancy between the two curves is within 1%. Table 4 shows the comparison of performance and accuracy between the FDM solver and the macromodels for the device.

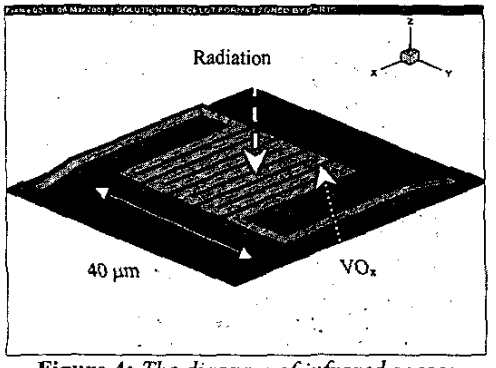

Figure 4: *The diagram of infrared sensor*

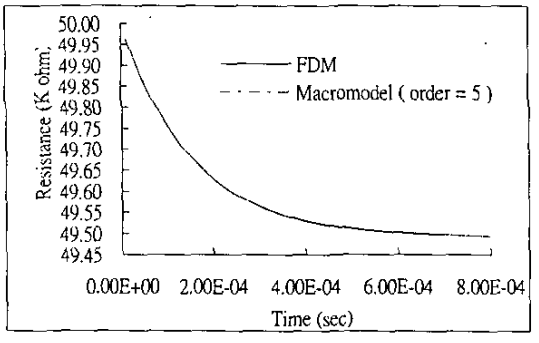

Figure 5: *Comparison between FDM and macromodel results: electrical resistance vs. time when the infrared imager pixel absorbs heat.*

	Simulation time (sec)	Speed-up factor	Error (%)
MOR order = 3	0.44	$3x10^4$	0.397
MOR order = 5	3.37	$4x10^3$	0.397
FDM	12421		N/A

Table 4: *The performance comparison of FDM solver and macromodels.*

4. Conclusion

A model order reduction technique for generating heat-transfer macromodels is presented in this work. Numerical analysis examples for simulating the transient heat transfer behaviors are demonstrated. The macromodel results are compared with the results from both FDM and commercial FEM solvers. The results of macromodels with order 3 or larger are accurate for the two examples demonstrated. The macromodel simulation performance is increased by at least 3 orders. The macromodels are compatible for system-level or circuit simulations. Experiment results of a thermal actuator are also in good agreement with the macromodel results.

ACKNOWLEDGMENT

This work is partially supported by the NSC (National Science Council, Taiwan, ROC) through the Grant contact No: NSC-91-2218-E-002-031.

REFERENCES

[1] Stephen D. Senturia, Microsystem Design, Kluwer Academic Publishers, 2001.

[2] F. Wang and J. White, "Automatic Model Order Reduction of a Microdevice using the Arnoldi Approach," ASME IMECE 98, DSC-Vol. 66, pp527-530.

[3] A. Odabasioglu, el. al., "PRIMA," IEEE Transaction on Computer-Aided Design of Integrated Circuits and Systems, Vol. 17, No. 8, August 1998.

[4] Y.-J. Yang, et. al. "Modeling Gas Damping and Spring Phenomena In MEMS With Frequency Dependent Macro-Models," IEEE MEMS 2001.

[5] A. F. Mills, Heat Transfer, Richard D. IRWIN, INC., 1992.

[6] Arieh Iserles, A First Course in the Numerical Analysis of Differential Equations, Cambridge University Press 1996.

[7] CoventorWare ANALYZER Tutorials, version 2001, Covertor, Inc., 2001.

[8] MUMPS Design Handbook

[9] Q.A. Huang, N.K.S. Lee, "Analysis and design of polysilicon thermal flexure actuator", Journal of Micromech. Microeng, vol 9, p 64-70, 1999.

[10] Jeffrey T. Butler, Victor M. Bright, William D. Cowan, "Average power control and positioning of polysilicon thermal actuators," Sensors and Actuators A: Physical, Volume: 72, Issue: 1, pp. 88-97, January 8, 1999.

[11] B. E. Cole, R. E. Higashi, R. A. Wood, "Monolithic Two-Dimensional Arrays of Micromachined Microstructures for Infrared Applications," Proc. IEEE, vol.86, no.8, pp.1679-1686, 1998.